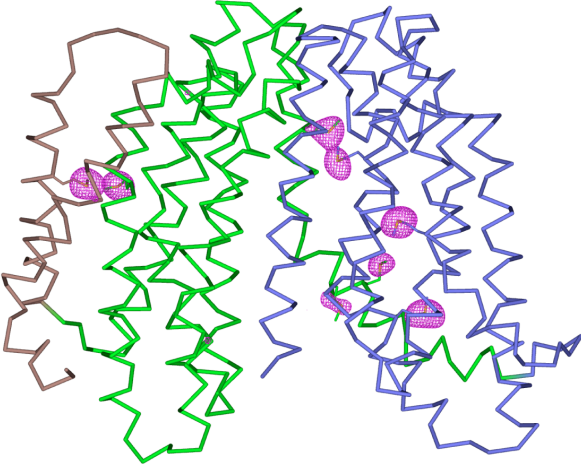
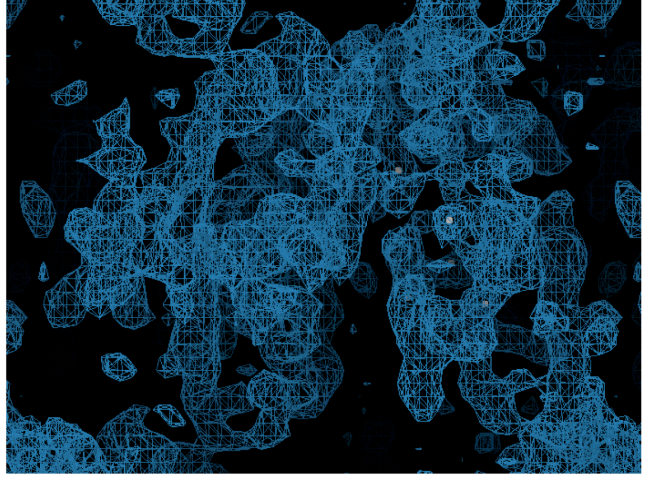
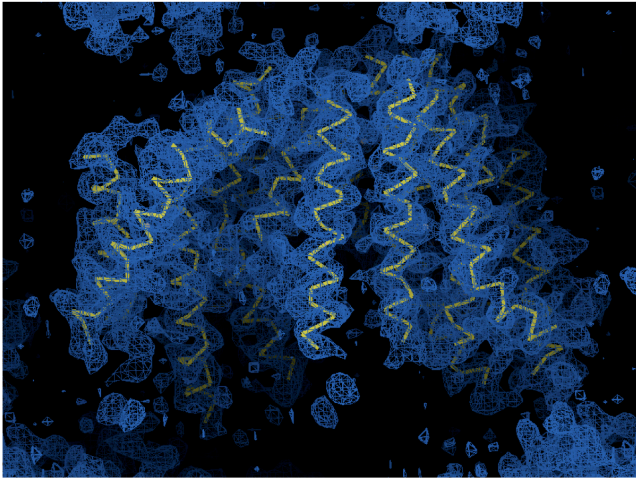
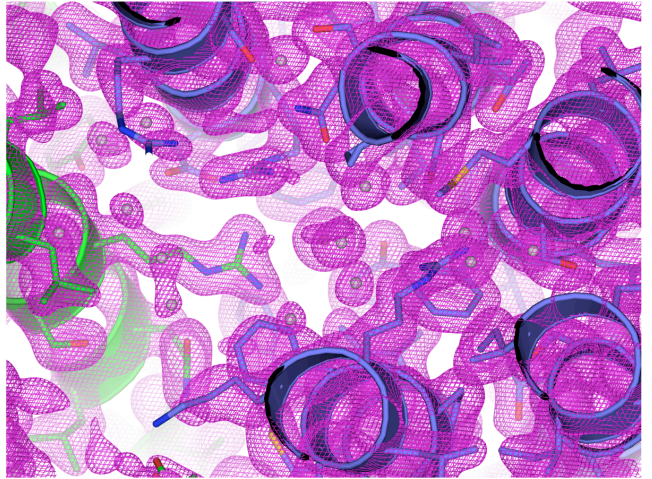
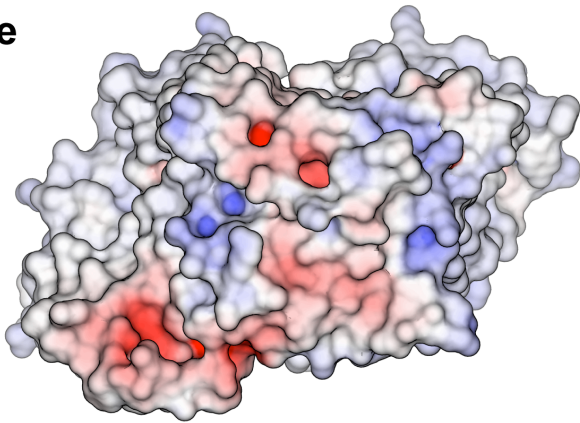
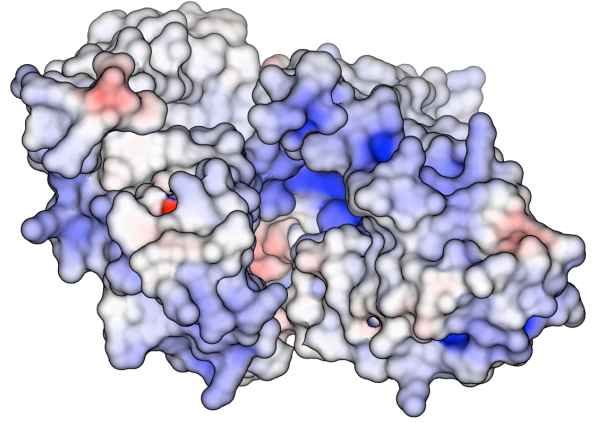


a**b****c****d****e**

Extracellular view

 \rightleftharpoons
 180°


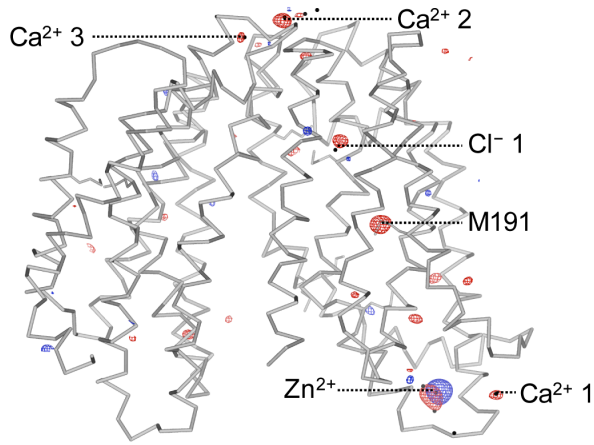
Intracellular view

Supplementary Figure 1

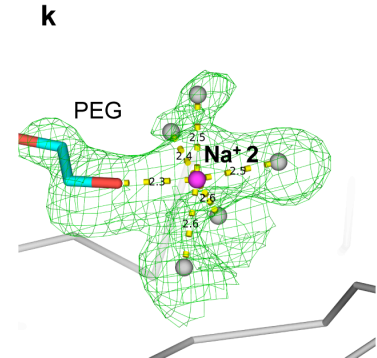
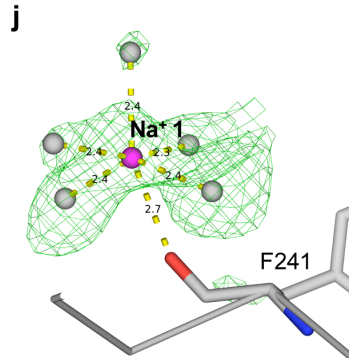
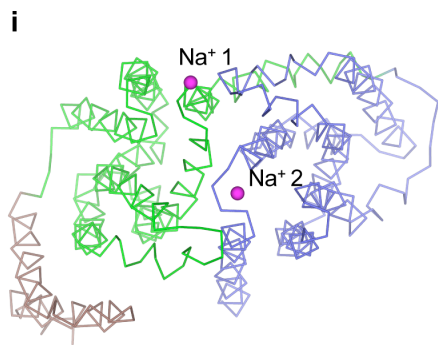
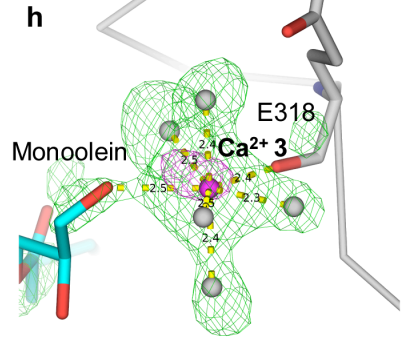
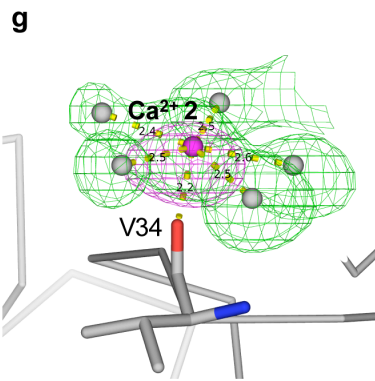
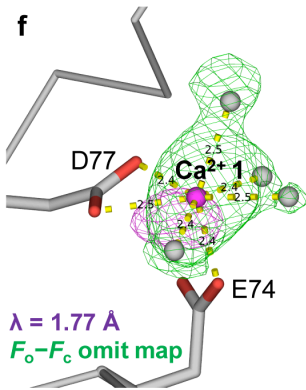
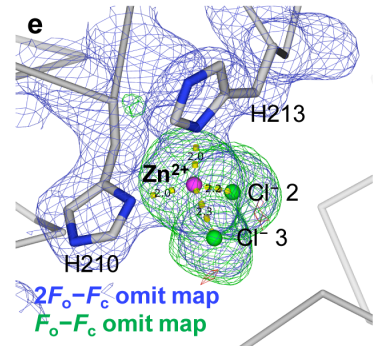
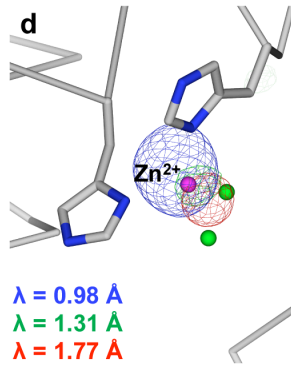
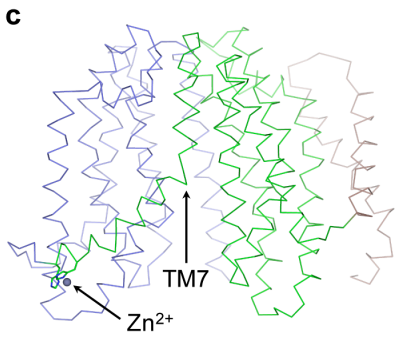
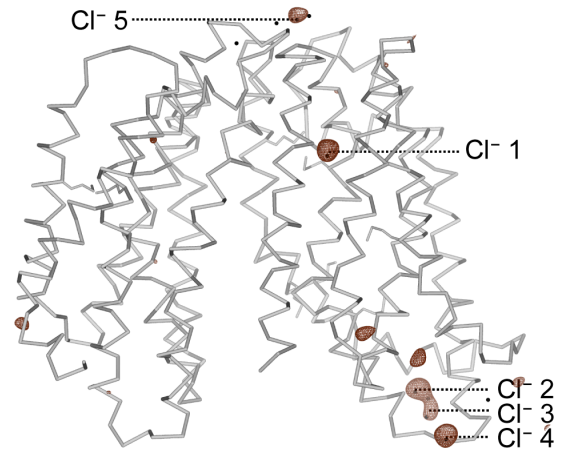
Experimental phasing of MurJ_{TA} from SeMet-substituted crystals

(a) Anomalous difference Fourier electron density peaks for selenium atoms are shown in magenta mesh contoured to 4σ . The map was calculated from the SeMet data up to 3.5 Å resolution. **(b)** Initial density-modified SAD map calculated from the SeMet data up to 5.0 Å resolution without any model phases. **(c)** Phase-extended electron density map calculated from the SeMet data up to 3.5 Å resolution, shown here with the working model consisting of α -helical fragments. **(d)** The $2F_o - F_c$ electron density map calculated from native data up to 2.0 Å resolution with the final refined model, shown here in close-up view around the chloride site in the central cavity. The map is contoured to 1.0σ . Water molecules are shown as gray spheres. **(e)** Electrostatic surface of MurJ_{TA}. Electrostatics are shown from -10 kT (red, anionic) to +10 kT (blue, cationic). The positive-inside electrostatics supports the inward-facing topology.

a Native ($\lambda = 0.98 \text{ \AA}$, $\lambda = 1.77 \text{ \AA}$)



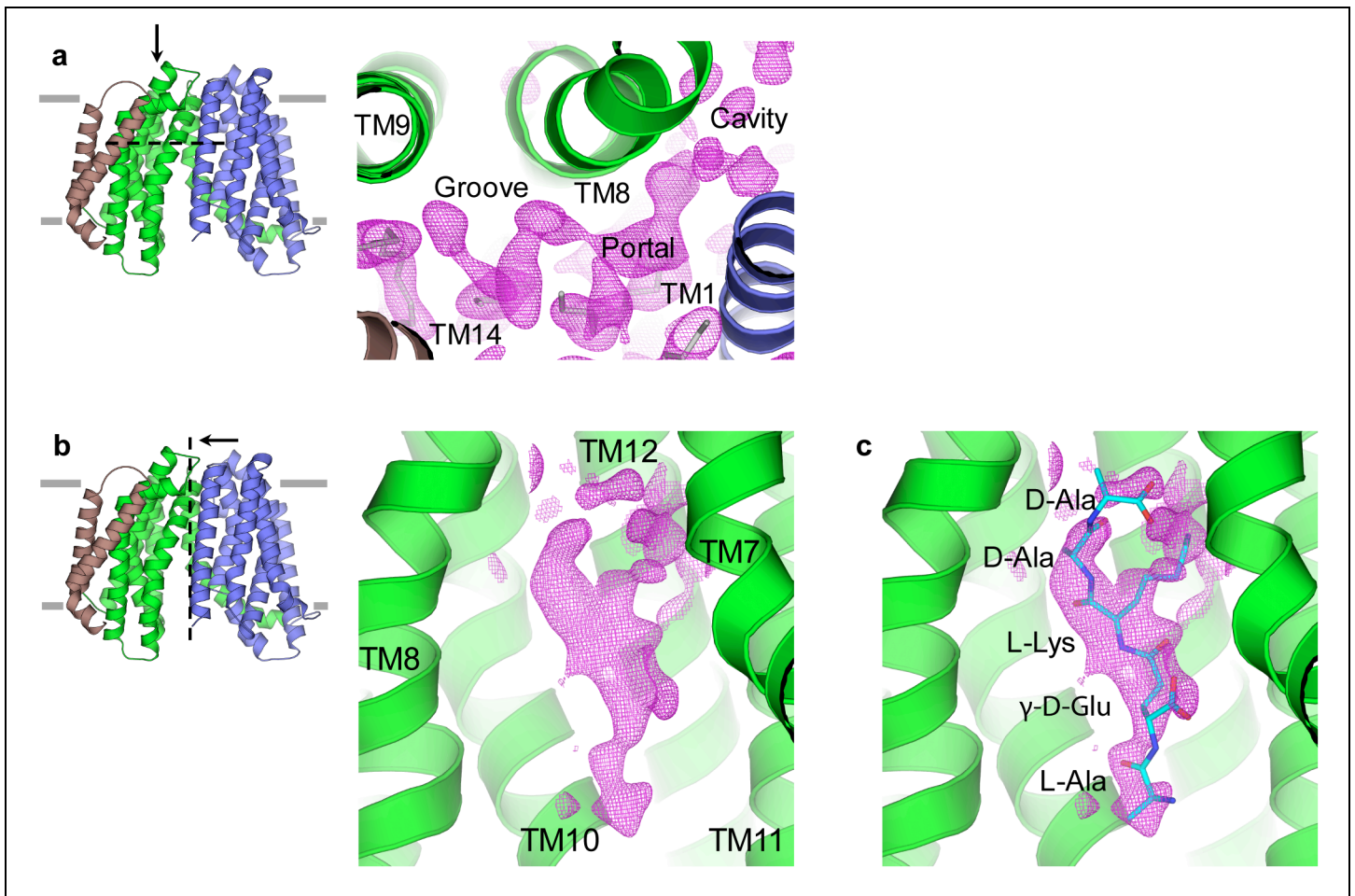
b Bromide soak, $\lambda = 0.92 \text{ \AA}$



Supplementary Figure 2

Cl^- , Zn^{2+} , Ca^{2+} , and Na^+ sites were deduced by anomalous scattering experiments and coordination geometry

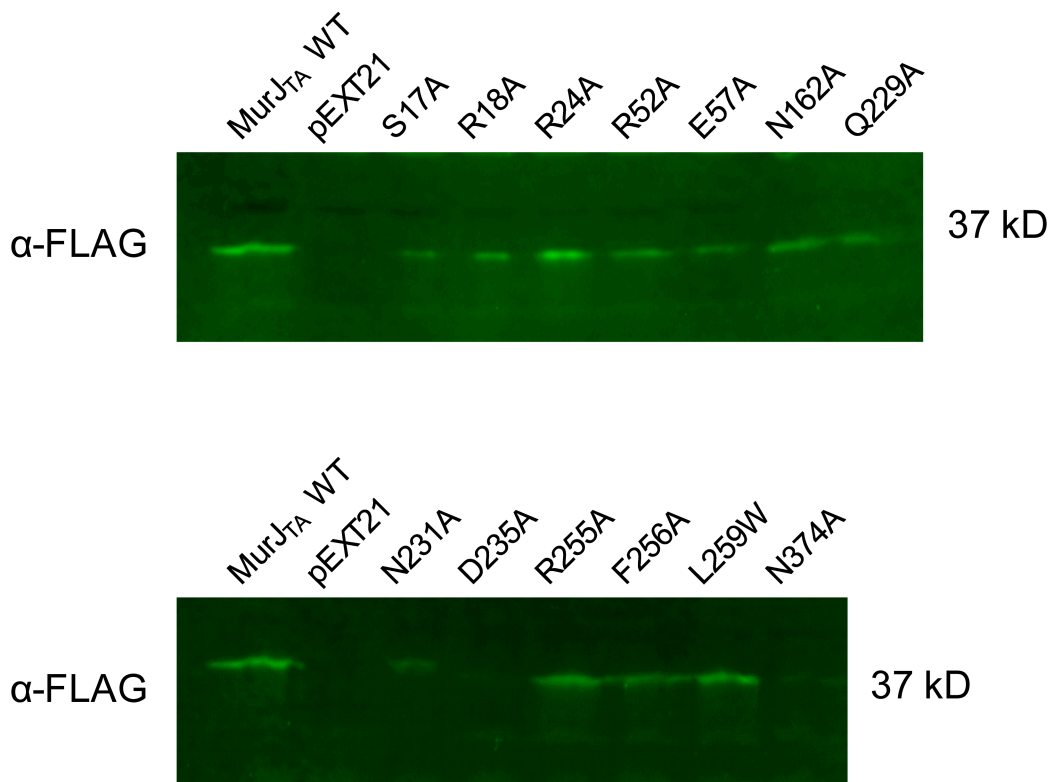
(a) Putative ion sites were first located by anomalous scattering experiments at $\lambda = 0.98 \text{ \AA}$ (blue mesh) and $\lambda = 1.77 \text{ \AA}$ (red mesh). Both anomalous difference Fourier (ADF) maps were calculated to 3.5 \AA resolution and contoured to 3.8σ . (b) Cl^- sites were identified by ADF density peaks from Br-soaked crystals ($\lambda = 0.92 \text{ \AA}$, brown mesh, calculated to 3.5 \AA resolution and contoured to 4.5σ). (c, d, e) A Zn^{2+} site strategically located at the start of TM7 was deduced on the basis of three factors. First, substantially higher ADF density was seen at $\lambda = 0.98 \text{ \AA}$ (blue mesh) than at $\lambda = 1.31 \text{ \AA}$ (green mesh) or $\lambda = 1.77 \text{ \AA}$ (red mesh), ruling out other common divalent metals such as Co^{2+} , Ni^{2+} or Fe^{2+} . All three maps were calculated to 3.5 \AA resolution and contoured to 5.5σ . Second, the Zn^{2+} ion displayed restrained tetrahedral coordination geometry to two histidines and two Cl^- ions, ruling out anions due to electrostatic repulsion. Third, the close coordination distance of 2.03 \AA to the nitrogen of both histidines also rules out many other common metal ions. (f, g, h) Ca^{2+} sites were identified on the basis of: (1) ADF density peaks ($\lambda = 1.77 \text{ \AA}$, magenta mesh, contoured to 3.5σ), and (2) characteristic 7-dentate pentagonal bipyramidal coordination geometry with 5 of the coordinating residues/waters arranged coplanar. The $F_o - F_c$ omit density is shown in green mesh. Electron density for the apex water coordinating Ca^{2+} site 2 above the pentagonal plane is not seen. (i, j, k) Putative Na^+ sites were deduced on the basis of the following: (1) lack of ADF density at $\lambda = 1.77 \text{ \AA}$, (2) octahedral coordination geometry with 6 coordinating groups, and (3) coordination distances of around 2.4 \AA . The height of the $F_o - F_c$ omit density (green mesh, contoured to 2.2σ) peaks for Na^+ sites 1 and 2 were respectively 4.2 and $>8 \sigma$. All omit maps were calculated from native data to 2.0 \AA resolution while omitting the respective non-protein atoms. Unless stated otherwise, $2F_o - F_c$ maps are contoured to 1.5σ , while $F_o - F_c$ maps are contoured to 3.0σ .



Supplementary Figure 3

Unmodeled electron density peaks in the portal and central cavity

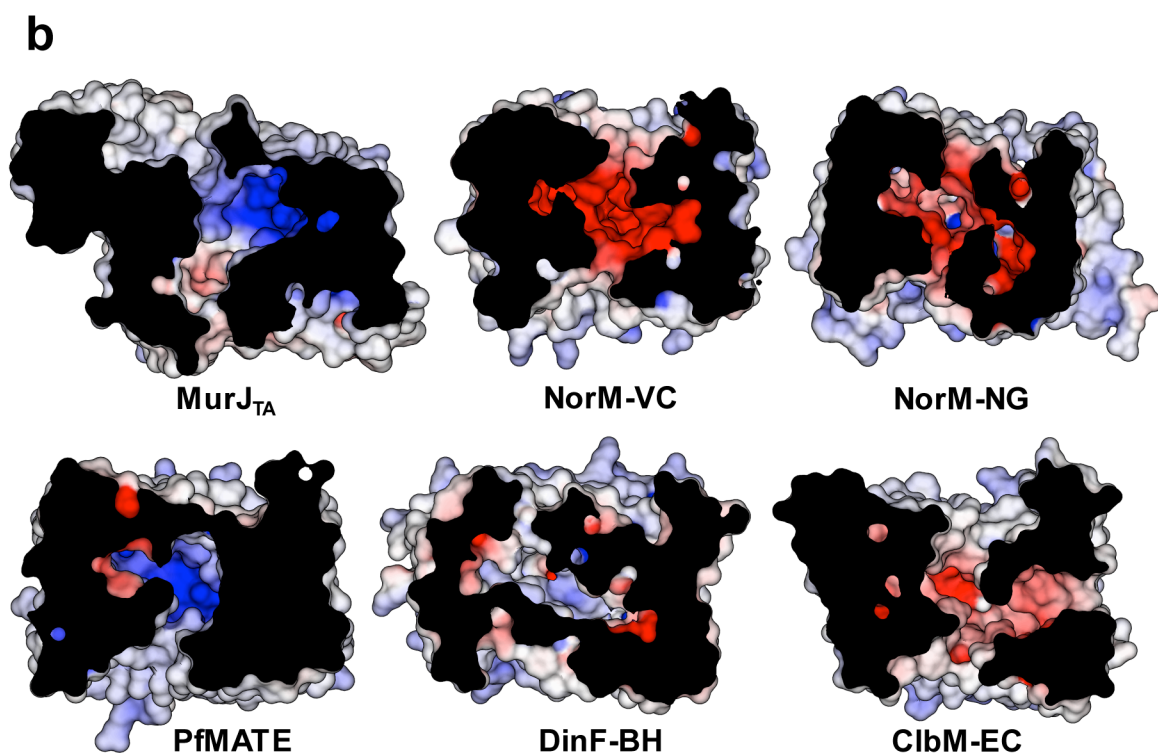
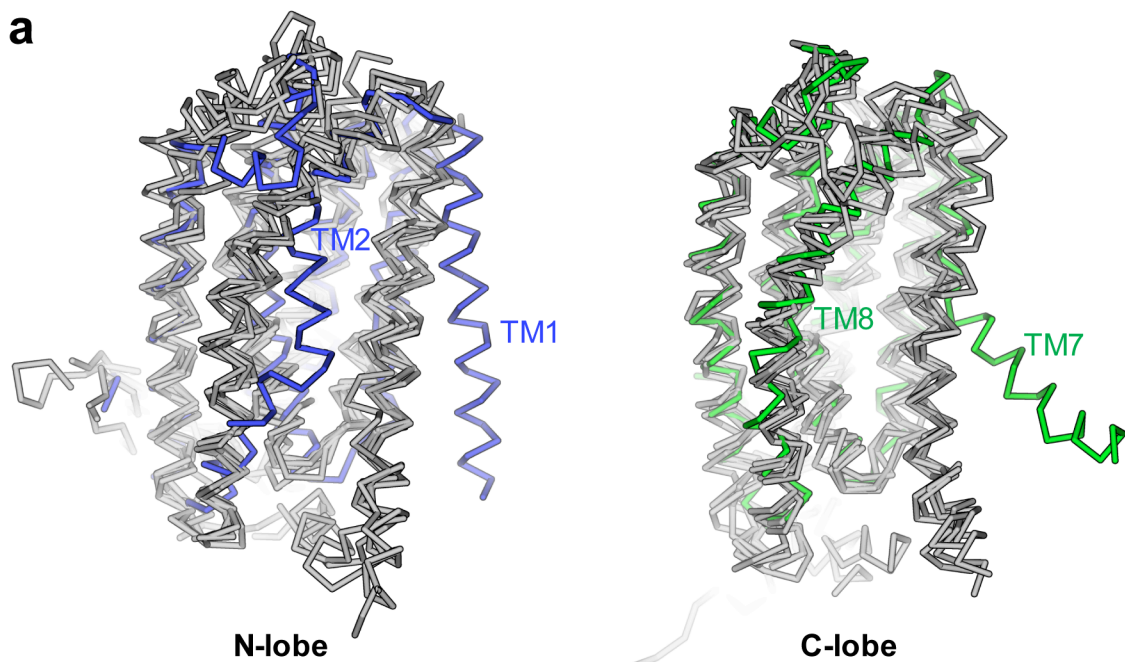
(a) The protein is sectioned on the dotted plane and viewed from the periplasm (along the direction of the arrow) to visualize the portal. The non-protein $2F_o - F_c$ electron density peaks are shown as magenta mesh, contoured to 0.7σ with the protein electron density masked. Gray sticks denote monoolein molecules. **(b)** The protein is sectioned and viewed from the right to visualize the distal site of the central cavity. The $2F_o - F_c$ electron density peaks are contoured to 0.7σ and carved 2.0 \AA from the pentapeptide model. **(c)** Model of the pentapeptide (L-Ala- γ -D-Glu-L-Lys-D-Ala-D-Ala) built into the density in panel b, but which was not used for refinement.



Supplementary Figure 4

Western blot of total membrane fractions from NR1154 cells transformed with pEXT21 encoding either wild-type (WT) or mutant MurJ_{TA}

MurJ_{TA} proteins carrying a C-terminal FLAG tag were expressed by the addition of 0.1 mM IPTG in the presence of arabinose. All of the mutants expressed with the exception of mutants D235A and N374A (image is representative of n = 3, technical replicates). There is no correlation between expression levels and complementation outcomes as long as the proteins are expressed: the lowest expression level was observed for the N231A mutant, which clearly complements MurJ_{EC}, while the highest expression level was observed in R24A, which clearly fails to complement. MurJ_{TA} (55 kD) migrates at an apparent molecular weight of 37 kD on a 10% SDS-PAGE gel.



Supplementary Figure 5

MurJ_{TA} is strikingly different from canonical MATE transporters, especially in TMs 1/2/8 as well as in cavity electrostatics

(a) Structural alignment between MurJ_{TA} (colored) with MATE transporters (gray) performed for individual lobes split at the start of TM7.

with TMs 13 and 14 removed. Structural differences are especially pronounced at TMs 1 and 2, while TM8 of MurJ_{TA} contains a segment that deviates from the α -helical geometry observed in MATE structures. The divergence at TM7 is likely a result of the inward-facing conformation of MurJ_{TA} as compared to the outward-facing conformations of the MATE transporters. Structures of MurJ_{TA} (PDB ID:5T77), PfMATE (3VVN), NorM-VC (3MKT), NorM-NG (4HUK), DinF-BH (4LZ6), and ClbM-EC (4Z3N) were used for the alignment.

(b) Surface charge differences between MurJ_{TA} and other MATE transporters. Surface electrostatics for MurJ_{TA} (PDB ID: 5T77) and MATE transporters NorM-VC (3MKT), NorM-NG (4HUK), PfMATE (3VVN), DinF-BH (4LZ6), and ClbM-EC (4Z3N) were calculated by the APBS plugin in PyMOL. The cavities of MurJ_{TA} and PfMATE are primarily cationic, in contrast to the strongly anionic cavities of NorM-VC, NorM-NG and ClbM-EC. The cavity of DinF-BH appears to have both weakly cationic and anionic patches.